Monthly Notices
of the
ROYAL ASTRONOMICAL SOCIETY

MNRAS **433,** 3364–3372 (2013) doi:10.1093/mnras/stt1024
Advance Access publication 2013 June 29

Synchrotron and inverse-Compton emission from radio galaxies with non-uniform magnetic field and electron distributions

M. J. Hardcastle⋆

School of Physics, Astronomy and Mathematics, University of Hertfordshire, College Lane, Hatfield AL10 9AB, UK

Accepted 2013 June 3. Received 2013 June 3; in original form 2013 March 21

ABSTRACT

I investigate the effect of non-uniform magnetic fields in the extended structures of radio galaxies on the observed synchrotron and inverse-Compton emission. On the assumption of an isotropic field, with a given power spectrum and a Gaussian distribution of the Cartesian components of the magnetic field strength, I derive a simple integral that can be used numerically to calculate the synchrotron emissivity from any electron population. In the case of power-law spectra, I show that it is possible to estimate the difference between the synchrotron emissivity from a region with such a field and that from the commonly assumed arrangement where B is constant everywhere, though fully tangled, and that this difference is small, though it increases if the electron energy density scales with the field. An aged electron spectrum in such a field produces a characteristic curved synchrotron spectrum which differs significantly from the classical Jaffe–Perola spectrum, and I discuss some effects that this might have on standard spectral age fitting. Finally, I show that inverse-Compton scattering of the cosmic microwave background is only moderately affected by such a field structure, with the effects becoming more important if the electrons follow the field. Magnetic field estimates in the literature from combined synchrotron and inverse-Compton modelling will give reasonable estimates of the mean magnetic field energy density if the field is non-uniform but isotropic.

Key words: radiation mechanisms: non-thermal – galaxies: active – radio continuum: galaxies.

1 INTRODUCTION

In order to estimate physical conditions in the extended components of radio galaxies (jets, hotspots and lobes) from the observed synchrotron and inverse-Compton emission (e.g. Hardcastle et al. 2004; Croston, Hardcastle & Birkinshaw 2005; Kataoka & Stawarz 2005), some simplifying assumptions must be made. In inverse-Compton modelling, in particular, it is typically assumed that the electron number density as a function of electron energy E [hereafter $N(E)$] is spatially uniform, and that the magnetic field strength in the region of interest (e.g. a jet, lobe or hotspot) can be characterized by a single value of B, where the magnetic field is assumed to be fully tangled on scales much smaller than the scale of interest.

These assumptions are clearly not valid in detail. It has been known for many years that the radio (synchrotron) emission from lobes and plumes shows complex fine ('filamentary') structure on a range of scales (e.g. Fomalont et al. 1989; Carilli et al. 1991; Swain, Bridle & Baum 1998; Laing et al. 2008). The existence of these structures proves that at least one of B and $N(E)$ is not spatially uniform within these structures. The fact that the radio spectra of different regions within the source are not identical (often attributed to 'spectral ageing', which will be discussed below in more detail) is generally taken to imply that $N(E)$ varies with position [though see Katz-Stone, Rudnick & Anderson (1993) and Blundell & Rawlings (2000) for alternative views]. Finally, in a very few sources, observations of inverse-Compton emission in which the radio/X-ray ratio varies as a function of position (e.g. Isobe et al. 2002; Hardcastle & Croston 2005; Isobe et al. 2005; Goodger et al. 2008) also imply that at least one of $N(E)$ and B vary on large spatial scales, and, in conjunction with multifrequency radio observations, can be interpreted as showing that both must vary (Hardcastle & Croston 2005). Moreover, the generally smooth appearance of inverse-Compton emission from lobes when observed at high resolution (Hardcastle & Croston 2005) implies that the variations in physical conditions responsible for the filamentary radio structure are very unlikely to arise in $N(E)$ alone. Modelling of the synchrotron and inverse-Compton emission from lobes should therefore ideally take into account these variations in physical conditions. In this paper, I shall focus on two aspects of this modelling where non-uniform B and $N(E)$ are likely to be important: spectral ageing and inverse-Compton modelling.

'Spectral ageing' is the name given to the long-established technique of using changes in the observed synchrotron spectrum to infer the time since the particles in the region of interest were last accelerated, and thus make inferences about the source age and/or

⋆ E-mail: m.j.hardcastle@herts.ac.uk

the lobe dynamics (e.g. Jaffe & Perola 1973; Burch 1977; Myers & Spangler 1985; Alexander & Leahy 1987; Carilli et al. 1991; Liu, Pooley & Riley 1992; Mack et al. 1998; Murgia et al. 1999; Jamrozy et al. 2008). If $N(E)$ is initially a power law in energy as a result of the acceleration process, then at some later time $t > 0$ we expect $N(E)$ to have a characteristic form depending on t. Since for synchrotron radiation the characteristic time-scale for energy losses goes as $1/E$, $N(E)$ at $t > 0$ will always be characterized by depletion of the highest energy electrons. The appropriate form of $N(E)$ depends on whether there is no pitch angle scattering of the electrons (Kardashev 1962; Pacholczyk 1970, hereafter KP) or effective pitch angle scattering (Jaffe & Perola 1973, hereafter JP). In the KP model, some very high energy electrons survive indefinitely because their pitch angles are very small and their energy losses negligible; thus the high-energy cutoff of the electron spectrum is that imposed by the original particle acceleration process, but there is a break in the electron energy spectrum when integrated over pitch angle at the point at which losses become non-negligible for electrons with larger pitch angles. Pitch angle scattering is more plausible a priori for realistic, turbulent magnetic field configurations because of the expected resonant scattering of particles on the field, which is effective on scales comparable to the Larmor radius of the electrons, and hence much smaller than the resolution of observations (see also discussion by Carilli et al. 1991). In the JP model, in which pitch angle scattering takes place, there is a critical energy, a function of t, above which there are no remaining electrons, and this in turn gives rise to an exponential cutoff in the synchrotron spectrum at high energies.

Both JP and KP models are in principle models of the shape (not normalization) of $N(E)$ and so are independent of our assumptions about electron number densities and magnetic field strengths, but in practice 'JP spectra' and 'KP spectra' are normally calculated and fitted to data on the assumption of a uniform magnetic field strength, and, moreover, it is often assumed that the field in which the particle energy spectrum has evolved is the same as that in which it is currently radiating. Early and important work on the problems with these assumptions was done by Tribble (1993), who showed numerically that a distribution of magnetic fields would give rise to synchrotron spectra that were significantly modified with respect to the JP and KP spectra, a point reiterated for different assumptions about the distribution of field strengths by Eilek & Arendt (1996). More recent work (e.g. Eilek, Melrose & Walker 1997; Kaiser 2005) has focused on analytical modelling of two-field systems, where ageing can take place in both fields but the emission is dominated by the high-field region; however, while this is analytically tractable and suffices to show that even simple variations of the field strength will give rise to observable effects on the synchrotron spectrum, the assumption of only two field strengths is a limitation of these models. With the new-generation radio telescopes providing much better frequency coverage of the synchrotron spectrum, it is timely to look again at modifications to the spectral ageing model.

The inferences drawn from inverse-Compton emission from lobes are also affected by inhomogeneous $N(E)$ and B. $N(E)$ of course affects inverse-Compton emission directly. For the simplest case, that of inverse-Compton scattering of the cosmic microwave background (CMB), the inverse-Compton emissivity depends only on the number density of electrons with $\gamma \approx 1000$, and since these are too low in energy to be depleted by loss processes in typical radio source lifetimes, the inverse-Compton emissivity simply depends on the low-energy normalization of $N(E)$. However, inverse-Compton emission is used to estimate B, by comparing the synchrotron emissivity, which depends on B, with the inverse-Compton emissivity, which does not: these estimates of a characteristic B may be very wrong in the presence of an inhomogeneous field. Synchrotron self-Compton (SSC) emission obviously depends on the distribution of $N(E)$ and B in a much more complicated way.

There are two possible ways to improve our understanding of the expected synchrotron and inverse-Compton properties of radio galaxies. In principle, the best approach would be to carry out full numerical modelling of the lobes, including all relevant physical processes that could affect the electron energy spectrum. This approach was pioneered, though with very low resolution and for axisymmetric jets, by Matthews & Scheuer (1990a,b). More recently, Tregillis, Jones & Ryu (2001) have carried out 3D magnetohydrodynamic (MHD) simulations including acceleration processes, and the state of the art for this type of work is represented by the type of code described by Mendygral, Jones & Dolag (2012), which can in principle give arbitrarily detailed inverse-Compton and synchrotron spectra as a function of position. The key advantage of such work is that the *relationship* between the particle and field populations should be realistic, with no simplifying assumptions necessary. The disadvantages are that such studies are computationally very expensive, their results depend on the input assumptions about the microphysics of, for example, particle acceleration and dissipation of magnetic fields, and they necessarily only sample a very small area of the parameter space that it is possible for radio-loud AGN to occupy. As a result, while such work is essential to provide a detailed understanding of these systems, it is difficult to abstract from it general methods for interpreting observational data.

In this paper, I take the complementary approach of using analytical calculations, supplemented by simple time-independent numerical modelling. I revisit some of the analytical and numerical calculations originally carried out by Tribble (1991, 1993, 1994), giving a clear statement of the analytic approach used and extending the numerical work using currently available computing power. In Section 2, I describe the general approaches used in the paper and discuss their applicability to real radio sources. In Section 3, I apply them to observations of aged synchrotron emission, noting in particular the important effect of structure on finite-sized regions on the observed spectral shapes, and in Section 4, I consider the consequences of the emission models developed in Sections 2 and 3 for inverse-Compton analyses. Discussion and prospects for further work are presented in Section 5.

2 THE METHODS

The analytical method used to describe synchrotron emission in a random magnetic field was described by Tribble (1991). The basic assumption he used was that the field is a Gaussian random field, i.e. that each component of the field at each point is drawn from a Gaussian distribution with mean zero and identical dispersion; this would be the case, for example, if the magnetic field structure is generated by homogeneous, isotropic turbulence.[1] In this case, the distribution of the magnitude of the magnetic field strength vector is a Maxwell–Boltzmann distribution. We can then consider the expected synchrotron emissivity for an arbitrary electron energy distribution. Let the electron energy spectrum be described by $N(E)$,

[1] In general, we expect MHD turbulence to be anisotropic (e.g. Cho & Lazarian 2003). My approach in this paper is to ignore anisotropy in the hope that this is a reasonable assumption for small enough regions of the source. Simulations of realistic MHD turbulence are beyond the scope of this paper.

where E is the energy of the electron and $N(E)\mathrm{d}E$ is the number density of electrons with energies between E and $E + \mathrm{d}E$. The single-electron emissivity as a function of frequency is given by (Longair 2010)

$$j(\nu) = \frac{\sqrt{3}Be^3 \sin\alpha}{8\pi^2\epsilon_0 cm_\mathrm{e}} F(x), \quad (1)$$

where B is the local magnitude of the magnetic field strength, e is the charge on the electron, ϵ_0 is the permittivity of free space, $F(x)$ is defined (Rybicki & Lightman 1979) as

$$F(x) = x \int_x^\infty K_{5/3}(z)\,\mathrm{d}z \quad (2)$$

with $K_{5/3}$ the modified Bessel function of the order of 5/3, and x is a dimensionless function of the frequency, field strength and energy:

$$x = \frac{\nu}{\nu_c} = \frac{4\pi m_\mathrm{e}^3 c^4 \nu}{3eE^2 B \sin\alpha}. \quad (3)$$

If we further assume that the pitch angle distribution is known (the standard assumption being that the electron population is isotropic, i.e. $p_\alpha = \frac{1}{2}\sin\alpha$), then we can write down an integral that gives the emissivity from the entire population at a given frequency:

$$J(\nu) = \int_0^\infty \int_0^\pi \int_{E_\mathrm{min}}^{E_\mathrm{max}} \frac{\sqrt{3}Be^3 \sin\alpha}{8\pi^2\epsilon_0 cm_\mathrm{e}} F(x) N(E) p_\alpha p_B \mathrm{d}E\,\mathrm{d}\alpha\,\mathrm{d}B \quad (4)$$

(cf. Eilek & Arendt 1996), where p_α and p_B are the probability distributions of the pitch angle α and the magnetic field strength B, respectively. As noted above, p_B for a Gaussian random field is the Maxwell–Boltzmann distribution, which we can write in a general form with a parameter a:

$$p_B = \sqrt{\frac{2}{\pi}} \frac{B^2 \exp(-B^2/2a^2)}{a^3}. \quad (5)$$

It is convenient to consider a field with a given mean magnetic field energy density, for which

$$\int B^2 p_B \mathrm{d}B = B_0^2 \quad (6)$$

which sets the value of the parameter $a = B_0/\sqrt{3}$.

Equation (4) can then be integrated – in the general case, numerically – over the known electron, pitch angle and magnetic field distributions to give a synchrotron spectrum. This is the method used by Tribble (1991) and, although not explicitly stated, Tribble (1993) must have used numerical integration of a version of equation (4).

Tribble (1994) described a numerical method, which would be expected to give the same results but which allows visualization of the synchrotron-emitting region rather than merely a calculation of its total emissivity, in which a box of random magnetic field is generated and the emissivity of each cell can be calculated. A general method for generating a random magnetic field with particular statistical properties was described by Tribble (1991). The same methods were used by Murgia et al. (2004, hereafter M04), modified to generate a magnetic field that might be appropriate for a turbulent cascade, and I closely follow the approach of M04 in what follows. Specifically, I generate the three components of the Fourier transform of the magnetic vector potential $\tilde{\boldsymbol{A}}(k)$ by drawing their complex phases from a uniform distribution and their magnitudes from a Rayleigh distribution whose controlling parameter σ ($|A_k|$ in the notation of Murgia et al.) depends on the wavenumber k as $\sigma = k^{-\zeta}$ between minimum and maximum wavenumbers k_min and k_max and is taken to be zero elsewhere. (In the numerical realizations that follow, I take $k_\mathrm{min} = 1$ and k_max to be the maximum value possible for the computational box used, so that the largest possible range of spatial scales is present in the models.) The Fourier transform of the magnetic field is then

$$\tilde{\boldsymbol{B}}(k) = i\boldsymbol{k} \times \tilde{\boldsymbol{A}}(k),$$

and I take the inverse three-dimensional Fourier transform of the three components of this, using code provided by the Fastest Fourier Transform in the West (FFTW) library, to find the real values of the components of the magnetic field vector $\boldsymbol{B}$, which are then renormalized to physical units. (For most of the runs used in this paper this is done using a 512 × 512 × 512 box.) This process, of course, gives rise to a Gaussian random field with zero mean, and the power spectrum $|B_k|^2 \propto k^{-(\zeta-2)}$ (M04).

To compute the synchrotron emissivity from the box, I use the method suggested by equation 22 of M04: that is, the effective magnetic field is taken to be the component perpendicular to the line of sight (which I take to be the z-direction of my Cartesian coordinates), so that $B_\perp = |\boldsymbol{B}| \sin\theta = B\sin\theta$. Since only electrons with pitch angles $\alpha = \theta$ contribute non-negligibly to the resulting radiation, this means that the single-electron critical frequency is everywhere proportional to $B_\perp E^2$. For speed, rather than numerically integrating over the electron energy density at every point in the grid, I compute the emissivity for a single value of $B_\perp$ for all required frequencies (using equation 4 but with p_B and p_α as delta functions), fit a cubic spline to it and then scale its normalization and base frequency using the values of $B_\perp$ and B appropriate to each cell.

An example of the projected synchrotron emissivity for such a magnetic field configuration (assuming a power-law electron energy spectrum with $N(E) \propto E^{-p}$: see below) is shown in Fig. 1; here, we assume a uniform electron density throughout the box.

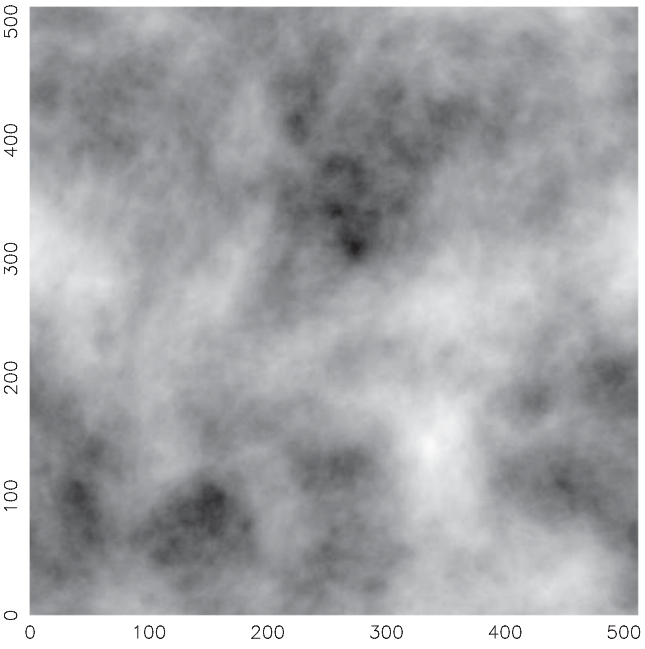

Figure 1. Synchrotron surface brightness from a spatially uniform ($s = 0$) power-law electron energy distribution and a spatially varying field as described in the text. Magnetic field with $\zeta = 5.667$, $k_\mathrm{min} = 1$ and $k_\mathrm{max} = 256$ is generated in a 512 × 512 × 512 box and the synchrotron emissivity projected along the z-axis. Lighter shades of grey indicate brighter regions; the scale is logarithmic with 0.89 dex between the brightest and faintest regions.

The appearance of the synchrotron emission from the region is clearly expected to be strongly dependent on the power spectrum used for the vector potential, i.e. on $k_{\rm min}$, $k_{\rm max}$ and ζ; it will also depend on the electron energy spectrum. One way of characterizing the synchrotron emission is to find its power spectrum: Eilek (1989) showed that a given power spectrum of the magnetic field translates into a particular two-dimensional power spectrum of the observed emission. Taking the two-dimensional Fourier transform of the projected emission and averaging its amplitude in radial bins to find the power on each spatial scale, I find that, as expected, a power law is recovered, with the amplitude going as k^{-n} where $n \approx \frac{2}{3}(\zeta - 3)$ for flat electron energy spectra ($p \approx 2$); there is only a very weak dependence on the electron energy index p, in the sense that higher values of p give rise to higher values of n. Carrying out the same procedure on some high-quality radio images, I find that power laws for the amplitudes of the observed synchrotron emission from well-resolved bright radio lobes have $n \approx 2$ in the range in which they are well described by a power law in k (which in practice is a range of scales starting significantly below the size scale of the lobes and ending significantly above the nominal spatial resolution), so that we should adopt $\zeta \approx 6$ to reproduce these. In what follows, I take a standard value of $\zeta = 5.667$, as used in Fig. 1, since this corresponds to a Kolmogorov spectrum for B. The fact that the observed properties of radio lobes are consistent with a simple model of magnetic turbulence together with a uniform electron energy spectrum gives us some confidence that the model used here is at least somewhat relevant to real systems.

What is of course missing from the numerically modelled synchrotron-emitting regions is any of the large-scale filamentary structure seen in real radio lobes. There are two reasons for this: first, the simulated region cannot, because of the way it is constructed, have any contribution from structures larger than the half-size of the box; secondly, the most striking of the filamentary structures are almost certainly a result of the large-scale internal dynamics of the lobes, and are a symptom of the processes that drive the turbulence rather than of the turbulence itself. I do not regard this as a serious problem since the only modelling I intend to carry out will be of regions small enough that the electron energy spectrum does not vary significantly across them; that is, the models should be taken to represent regions much smaller than the characteristic size of the lobes (with the caveat that, of course, we have few observational constraints on the properties of magnetic turbulence on those scales).

3 SYNCHROTRON SPECTRA

3.1 Power-law electron spectra

The synchrotron spectrum of a region containing a non-uniform magnetic field, for a given electron energy distribution, can now be investigated. I choose to restrict this to the situation where the electron energy spectrum is the same, apart from normalization, at all points in space: this is reasonable if the diffusion time for electrons throughout the region is much shorter than the loss time, so that, averaging over loss times, all electrons probe the same mean magnetic field strength. [See Tribble (1993) and Eilek et al. (1997) for modelling in which this is not the case.] Since there is some evidence that $N(E)$ does vary on the largest scales, these models are not applicable on those scales.

We can begin by considering a power-law distribution of electrons, $N(E) = N_0 E^{-p}$. In this situation, it is clear from the standard arguments that we still expect a power-law synchrotron spectrum with the usual frequency dependence, $J(\nu) \propto \nu^{-(p-1)/2}$. Only the normalization can change. In fact, for the case where we have a uniform $N(E)$ independent of B, we can see that if the mean squared magnetic field strength is the same, B_0^2, the *total* electron energy loss rate to synchrotron emission in the region must be the same, and as the spectral shapes are the same except at the end points of the power law, the normalizations should be essentially identical. Another way of seeing this is to integrate the standard power-law emissivity approximation,

$$J(\nu) = K N_0 \nu^{-\frac{(p-1)}{2}} B^{\frac{(p+1)}{2}}, \tag{7}$$

where K is a constant, over the distribution of magnetic field strengths, obtaining

$$\int J(\nu) p_B \, {\rm d}B = \frac{2}{\sqrt{\pi}} \left(\frac{2}{3}\right)^{\frac{p+1}{4}} \Gamma\left(\frac{p+7}{4}\right) K N_0 \nu^{-\frac{(p-1)}{2}} B_0^{\frac{(p+1)}{2}}, \tag{8}$$

where the leading numerical term differs from unity by only a few per cent over a physically reasonable range for p (2–3); that is, the emissivity from a Maxwell–Boltzmann distribution of field strengths is only very slightly different from that from $p_B = \delta(B - B_0)$, a fully tangled field with a constant magnetic field strength.

Somewhat more interesting is the case where the normalization of the electron energy spectrum (N_0) is not a constant in space. It is clear that if the variations in N_0 are uncorrelated with those in B, then there will be no effect on the synchrotron emissivity integrated over a sufficiently large volume – we simply replace the constant N_0 in the equations above with its mean value $\bar{N}_0$. More interesting is the case where the local normalization depends on the magnetic field strength. We may assume some general power-law relation,

$$N_0 \propto \left(\frac{B}{B_0}\right)^s, \tag{9}$$

where $s = 0$ corresponds to no dependence on B and $s = 2$ to what we could think of as 'local equipartition' – the energy density of the particles scales everywhere with that in the field. Eilek (1989) suggests that intermediate values of s, 1–1.5, might be reasonable in trans-sonic turbulence. Then, the ratio between the emissivity in this situation and that in the fully tangled, uniform-density, uniform-field case with the same mean magnetic field and particle energy density becomes

$$\frac{\int B^s B^{\frac{(p+1)}{2}} p_B \, {\rm d}B}{B_0^{\frac{(p+1)}{2}} \int B^s p_B \, {\rm d}B} = \left(\frac{2}{3}\right)^{\frac{p+1}{4}} \frac{\Gamma\left(\frac{s}{2} + \frac{p+7}{4}\right)}{\Gamma\left(\frac{s+3}{2}\right)}. \tag{10}$$

This is an almost linear function of s which goes from $\sim$1 at $s = 0$ to $\sim$1.5 at $s = 2$, more or less independent of p in the range discussed above. Thus, we expect the total emissivity in models in which the electron density follows the field strength to be up to a factor of 1.5 higher than in the uniform-density, constant-field-strength models for a power-law spectrum. We also expect the power spectrum of the resolved emissivity to have a steeper power-law index, since the effect of increasing s is to increase the contrast between the brightest and faintest regions of the map. In practice, this is a small effect, with the value of n increasing by only $\sim$0.1 for $s = 2$, $p = 2.2$.

Finally, it is important to note that the preceding analysis is for the idealized case where we integrate over an infinite volume. In real systems, and in particular in systems where a turbulent magnetic field power spectrum extends to the largest available scales,

as discussed in Section 2, there will be considerable scatter in the relationship between mean electron and magnetic field energy density on the one hand, and emissivity on the other. We return to this point below.

3.2 Aged spectra

We may now consider spectral ageing. I adopt the JP electron spectrum, i.e.

$$N(E) = \begin{cases} N_0 E^{-p}(1 - ECt)^{(p-2)} & E < 1/Ct \\ 0 & E \geq 1/Ct, \end{cases} \quad (11)$$

where C is the constant such that

$$\frac{\mathrm{d}E}{\mathrm{d}t} = -CE^2, \quad (12)$$

i.e. C takes account of both radiative and inverse-Compton losses:

$$C = \frac{4\sigma_T}{3m_e^2c^3}\left(U_{\rm IC} + U_{B,\rm loss}\right) \quad (13)$$

(Longair 2010), where $U_{\rm IC}$ is the energy density in photons and $U_{B,\rm loss} = B_{\rm loss}^2/2\mu_0$ is the energy density in the effective field seen by the radiating electrons over their post-acceleration lifetime, which in general will be different from the local B.

The JP spectrum is the only one of the two 'traditional' electron spectra discussed above that is reasonable to consider – as discussed in Section 1, the turbulent magnetic field that we impose would be expected to lead to effective scattering as long as there is structure in the magnetic field on scales comparable to the Larmor radius of the electrons. Such an electron energy spectrum is expected in a non-uniform magnetic field model if, as noted by Kaiser (2005), the electron diffusion coefficient is independent of energy – in this case, all electrons in a given volume can be taken to have the same average loss history, and we can adopt $B_{\rm loss} = B_0$. (This is also true, independent of the diffusion coefficient, if inverse-Compton losses dominate, i.e. $B_{\rm IC} \gg B_{\rm loss}$.)

This electron spectrum can then be used in equation (4) to compute the synchrotron emissivity (throughout this section of the paper we assume $s = 0$). Fig. 2 shows plots of the aged synchrotron spectrum for a Maxwell–Boltmann distribution of magnetic field strength, assuming a uniform electron density that does not depend on B (for simplicity I refer to these as Tribble–Jaffe–Perola, or TJP, spectra in what follows). To allow a concrete comparison to real synchrotron spectra, I set $B_0 = 1$ nT, $B_{\rm loss} = 1$ nT and $U_{\rm IC}$ appropriate for the $z = 0$ CMB; this is a regime appropriate for lobes of powerful radio galaxies in the local Universe. The age t is varied between 10^7 and 10^8 yr. Also plotted, for comparison, are the JP synchrotron spectrum appropriate for a single B-field value, $B = B_0$.

Several important points can be noted on this plot. First of all, we see that the spectral shape is significantly altered by the adoption of a Maxwell–Boltzmann distribution for B: the TJP spectrum cuts off at higher frequencies and curvature is visible over a wider frequency range. This is not at all surprising, since we can view these spectra

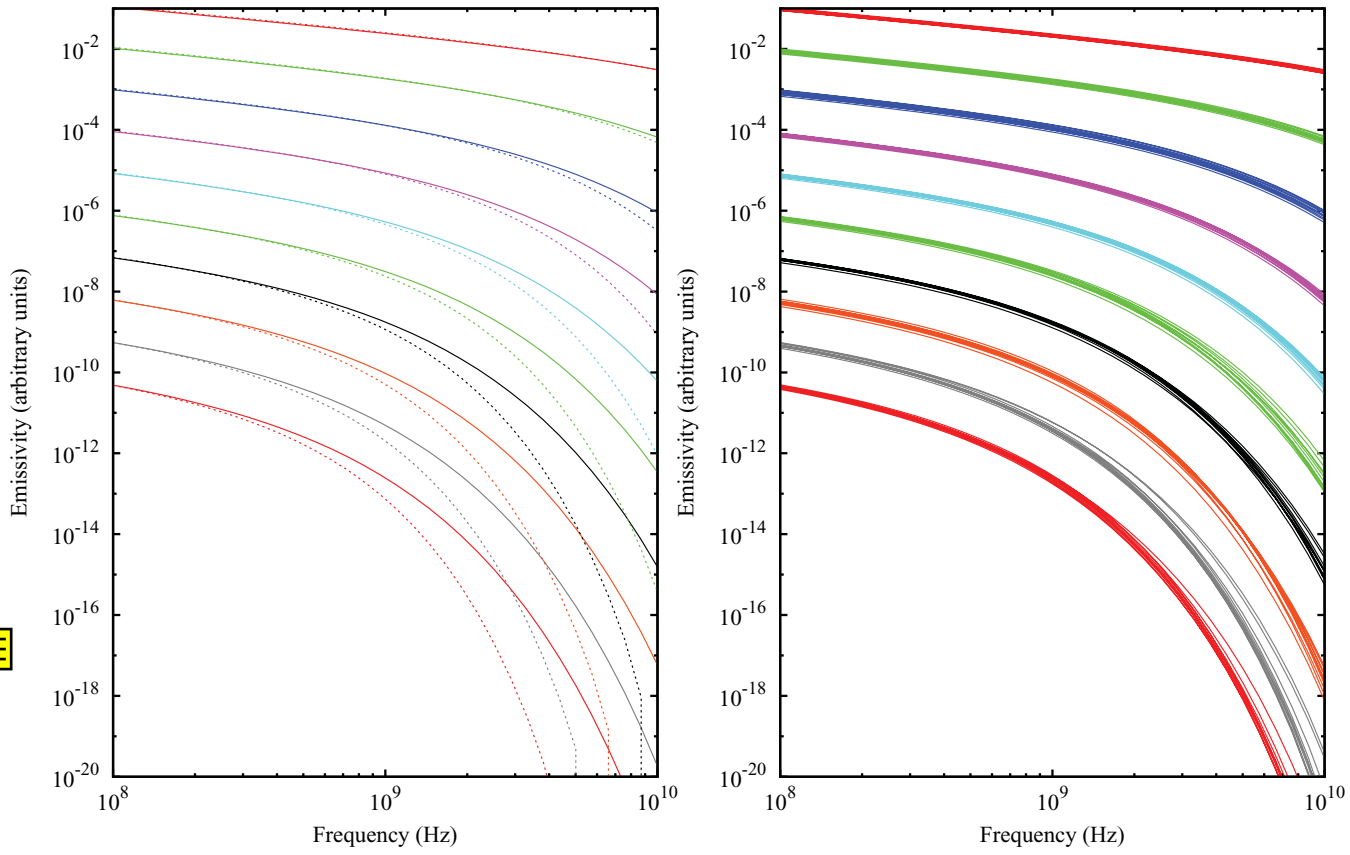

Figure 2. Aged spectra in TJP and classical JP models. Left: solid lines show the spectrum arising from numerically integrating the JP electron spectrum over the Maxwell–Boltzmann distribution of magnetic field strengths, with spectral ages of 10^7 (flattest, top), $2 \times 10^7, \ldots, 10^8$ yr (steepest, bottom) with $B_0 = 1$ nT. An order of magnitude in normalization is inserted between each curve. The dotted lines show the classical JP spectrum with a fixed magnetic field strength of 1 nT. Right: spectra from 10 numerical realizations of finite-sized regions containing JP electron spectra, showing the dispersion that arises from the magnetic field structure in such regions, with each colour corresponding to runs for the age values plotted in the left-hand panel.

as the weighted sum of many individual single-field JP spectra, with the break frequency for each being shifted according to equation (3). The spectra resemble the classical JP spectra in the sense that, unlike the case in KP spectra, the spectral index between any two frequencies ν_0 and $\nu_1 = C\nu_0$ gets monotonically steeper as ν_0 moves upwards in frequency. However, we also see that the spectra do not have the same shape as classical JP spectra either – a TJP spectrum matched to a single-frequency JP spectrum at high and low frequencies is more strongly curved at intermediate frequencies, and this excess curvature could in principle be used to distinguish between them. Sensitive observations spanning a broad frequency range, such as the ones that will soon be provided by combining data from the LOw Frequency ARray (LOFAR) and the Jansky Very Large Array (JVLA), will be needed to see if these models can be tested.

Secondly, we see that the normalization of the two spectra is very similar; this follows from the type of argument we used above to discuss power laws. Since the TJP extends to higher frequencies, we would expect its normalization to be slightly below that of the uniform-field spectrum, which is observed.

Finally, we see that in the realizations of the TJP spectra using the numerically modelled regions, plotted in Fig. 2 (right-hand panel), there is very substantial scatter, particularly in steep-spectrum regions. This comes about because the magnetic field structure that we have generated has its maximum power on scales comparable to that of the box itself – they are not simply a resolution effect, but show the real expected degree of scatter in a Gaussian random magnetic field with a power spectrum of the type we have chosen. We expect this to be a realistic description of regions much smaller than the lobe size, where the largest scale of surface brightness variation is larger than the region size, so long as the power spectral index ζ is not too flat. As the plots show, finite-size realizations (which is what we always see in practice) may differ significantly from the idealized spectra derived by integration of equation (4). In steep-spectrum regions of highly aged spectra, the dispersion in the predicted flux density can easily be an order of magnitude (and would be larger still for $s > 0$).

As pointed out by Tribble (1994), the emissivity for such an aged electron spectrum, for appropriately high frequencies, is a very strong function of magnetic field strength, because the local B determines the break frequency of the local synchrotron emissivity. It is a general prediction of models in which the observed filamentary structure is determined by magnetic field variation that the filamentary structures will become more prominent as we move to higher observing frequencies, or, equivalently, that brighter regions will have flatter spectra than fainter regions.

If real radio galaxies have spectra described by the TJP model, what are the consequences of the widespread fitting of the standard JP model with its assumption of a uniform magnetic field? One is obvious: for a given electron age, the TJP spectra cut off at higher frequencies, so we would expect JP models to underestimate the true spectral age. Although this effect is not large (Fig. 2), it is in the sense expected from the generally accepted conclusion that the spectral ages underestimate the dynamical ages of radio galaxies (e.g. Eilek 1996). Another consequence is slightly less obvious. Because the TJP models are more curved than the JP models at low frequencies, fitting a JP model over a finite frequency range, with the 'injection index' – i.e. the low-frequency spectral index – left as a free parameter, will tend to produce artificially high injection indices – the TJP model flattens more at frequencies below those that are observed than the JP model expects. The magnitude of the effect will depend on the frequencies used and the location of the spectral break with respect to them, and so is hard to quantify, but some simple tests suggest that the effect is not negligible. Users of the JP model should treat best-fitting injection indices with caution; however, see Harwood et al. (submitted), for an example where the TJP and JP models do not give significantly different answers.

4 INVERSE-COMPTON MEASUREMENTS

4.1 Scattering of the CMB

If the electron number density is constant, the results of Section 3.1 are good news for inverse-Compton estimates of magnetic field strength that involve scattering of an isotropic photon field such as the CMB. The emissivity from this process depends on the number density of low-energy electrons (e.g. $\gamma \sim 1000$ for scattering of CMB photons to keV X-ray energies) and therefore on the normalization of the electron energy spectrum, N_0. The magnetic field strength is then essentially estimated from synchrotron observations using equation (7) (in the case of a power law), so

$$B \propto \left(\frac{J(\nu)}{N_0}\right)^{\frac{2}{p+1}}, \tag{14}$$

where the assumption is that there is a single value of B throughout the region of interest.

As we saw in Section 3.1, replacing a single magnetic field strength B with a distribution of field strengths characterized by a mean squared field B_0^2 barely changes the normalization of the relationship between N_0 and synchrotron emissivity, $J(\nu)$ (equation 8). Therefore, magnetic field estimates derived in this way are good estimates of the mean field B_0. Even if we consider the case where the electron energy density scales with the field energy density ($s = 2$ in equation 9), we saw that the normalization of the $J(\nu)$–N_0 relationship changes at most by a factor of 1.5 (in the sense that more emission is produced for a given mean number density of electrons). The integrated inverse-Compton emissivity, which depends on the mean value of N_0, is unchanged in such models, and so the change in synchrotron emissivity would mean that the mean magnetic field strength would be overestimated by at most a factor of $\sim$1.3 (for $p = 2$). Similar results will hold for more complex spectra, such as the curved spectra of Section 3.2, though here additional systematic errors in the standard calculations will result from incorrect assumptions about the mapping between the electron energy spectrum and the synchrotron spectrum.

One interesting feature of inverse-Compton emission is that it is possible to test the class of models where the electron energy/number density scales with field strength (i.e. where $s > 0$ in equation 9); as noted above, these models have little effect on global properties of the synchrotron spectrum such as the power spectrum index. If $s > 0$, we expect to see structure in the inverse-Compton emission that will correlate with structure in the synchrotron emission – the correlation will not be perfect (since the emissivities in inverse-Compton and synchrotron are always different non-linear functions of the local magnetic field strength) but will be more apparent for high values of s. We can visualize this reasonably well, without doing a detailed calculation by assuming that the inverse-Compton emissivity scales as N_0; examples are given in Fig. 3. Sources that show bright, resolved inverse-Compton emission allow us to put constraints on the value of s (Goodger et al., in preparation).

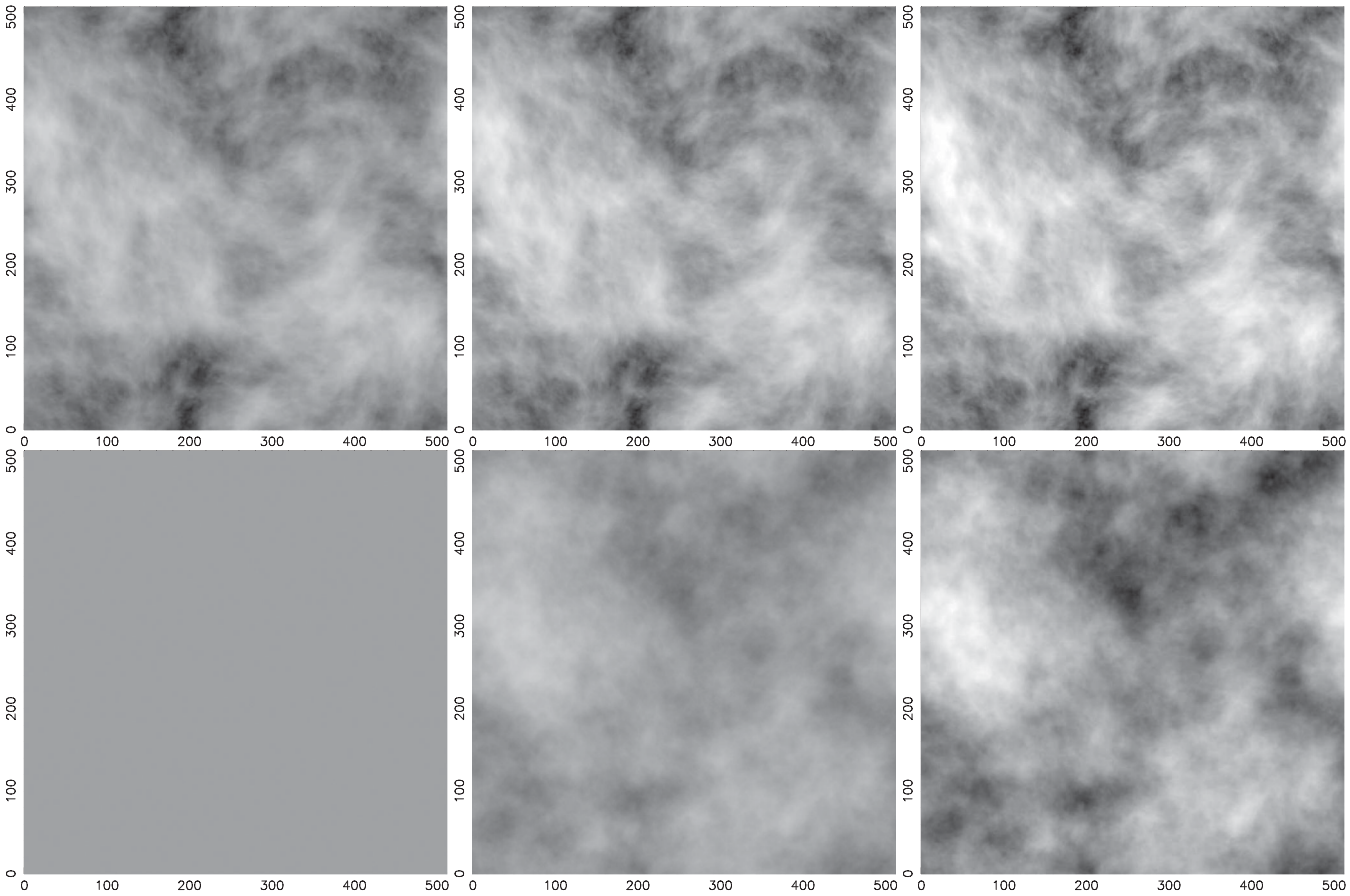

Figure 3. Synchrotron (top) and inverse-Compton (bottom) emission from the same magnetic field distribution, with the electron energy density dependence on the magnetic field strength increasing from left to right: the three panels show $s = 0$, 1 and 2, respectively. Grey levels are logarithmic and are the same for each set of images.

4.2 Synchrotron self-Compton

Synchrotron self-Compton (SSC) emission is a much more challenging problem, since the photon field is no longer isotropic and the spectrum from every illuminating point may be different. We expect the SSC emission from a region with variable magnetic field strength to be non-uniform even if the electron density is uniform. To calculate the SSC from our numerical models we need, in principle, to consider the illumination of every point by every other point, integrating the full anisotropic inverse-Compton kernel over the distribution of electrons and incoming photons. This is computationally very expensive, and so shortcuts of various sorts are normally taken to avoid having to do the full integration (e.g. Hardcastle et al. 2002; Hardcastle & Croston 2011). In order to get an estimate of the effects of inhomogeneous magnetic fields, I consider only power-law spectra, which has the effect that we need not consider a different synchrotron spectrum from each volume element, though I still take account of the anisotropic emissivity of synchrotron radiation. I treat anisotropic inverse-Compton scattering using the approach of Hardcastle et al. (2002), based on the inverse-Compton formulations of Brunetti (2000), which are integrated over the power-law photon and electron distributions, assuming scattering from a fixed radio frequency to 1-keV X-rays (i.e. well away from the Klein–Nishina regime). All of these simplifications reduce the computation for each pair of volume elements to a few simple operations, rather than any numerical integration. Even so, the N^6 dependence of execution time makes the use of 512^3 boxes, as in earlier parts of the paper, impossible, and the results in what follows are based on 100^3 boxes, which can be run in a few minutes on a moderate number of compute cores. (For consistency, I continue to use cubical boxes even though the geometry affects the emissivity for the SSC process, because of edge effects, and a cube is not a realistic shape for an astrophysical object – the scaling results should be the same whatever the shape we consider.)

We would expect that the mean SSC emissivity from a box where $s = 0$, so that the electron density is uniform, would be comparable to the emissivity for the case where both the electrons and field (and hence the synchrotron emissivity) are uniform, and this is indeed what we see: the SSC emissivity is not uniform in finite-sized realizations, because of the non-uniform synchrotron emissivity, but it is much less strongly structured than the synchrotron emissivity because photons from the whole volume illuminate every region. For $s > 0$, the results are expected to be more interesting, because now higher densities of electrons are concentrated in regions of higher photon energy density, and indeed we see that structure begins to appear in the inverse-Compton images (Fig. 4). The mean inverse-Compton emissivity also increases, by a factor of 1.3 for $s = 1$ and 1.6 for $s = 2$ – thus it tracks, rather closely, the increase in synchrotron emissivity discussed in Section 3.1, as we might expect (Fig. 5). The effect of such models would therefore be on average to increase both synchrotron and SSC emissivity, more or less in steps. Since for power-law SSC we know that

$$J_{\rm SSC} \propto N_0 J_{\rm synch} \tag{15}$$

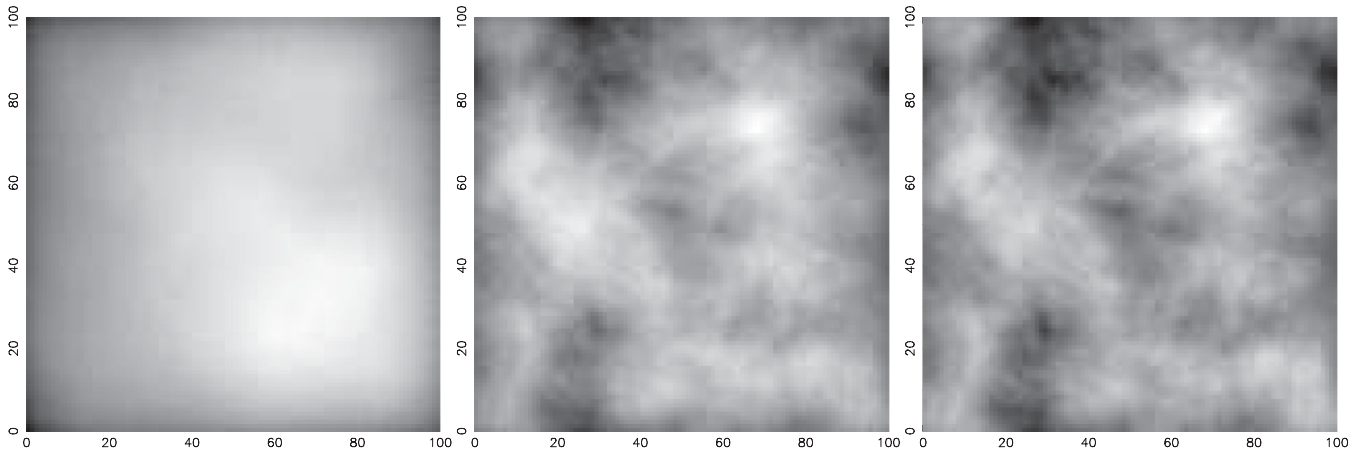

Figure 4. SSC emission from a 100^3 simulated box, on the assumption of, from left to right, $s = 0$, $s = 1$ and $s = 2$; all three boxes have the same magnetic field distribution. The dynamic range is allowed to vary (i.e. the greylevels are not matched) so that structure in the $s = 0$ image can be seen. The dynamic range of the three images (the ratio of surface brightness represented by white points to those represented by black points) is, respectively, 3.2, 7.4 and 14.5.

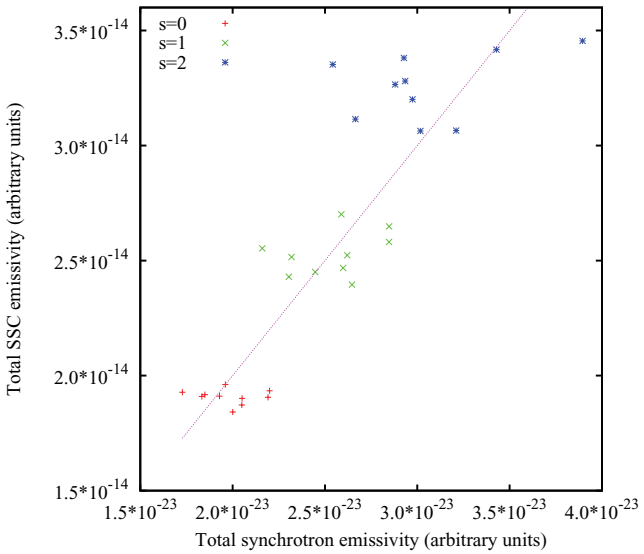

Figure 5. Total synchrotron and SSC emissivity for 10 realizations of 100^3 boxes with $s = 0$, 1 and 2. Both SSC and synchrotron emission increase as s increases, and the scaling is very nearly linear (for comparison, the purple line shows a linear scaling normalized by eye to pass through the data points). The scatter in the synchrotron emissivity is greater than that in SSC.

and so from equation (7)

$$B \propto \left(\frac{J^2_{\rm synch}}{J_{\rm SSC}} \right)^{\frac{2}{p+1}}, \qquad (16)$$

then the fact that $J_{\rm SSC}$ averaged over the volume scales roughly as $J_{\rm synch}$ means that, as with the CMB inverse-Compton, B-field estimates derived in the conventional way will be wrong only by a factor of $\sim$1.3 for $p = 2$, $s = 2$. In finite-sized regions, there will of course be scatter in both the synchrotron and SSC emission, but the former is dominant (Fig. 5). If the spectra have substantial curvature, as in the models of Section 3.2, then the dynamic range of the SSC images would be expected to increase significantly (particularly as high-frequency photons in the synchrotron emission are important for efficient SSC scattering to X-rays by low-energy electrons). We might also expect the SSC results to be somewhat dependent on the power spectrum of fluctuations, ζ.

As with the CMB inverse-Compton, we could in principle test for $s > 0$ by looking at the strength of the correlation between SSC and synchrotron surface brightness. However, most well-resolved lobes are unlikely to be dominated by SSC. One exception is Cygnus A (Hardcastle & Croston 2011) but X-ray inverse-Compton emission is only barely detected in this source against the thermal fore/background emission from the host cluster, and mapping it spatially will almost certainly require next-generation instruments.

5 SUMMARY AND CONCLUSIONS

The key points from the analysis presented in this paper are as follows.

(i) I have given an explicit formula (equation 4) for the synchrotron emissivity in a large region with a Gaussian random magnetic field – this was implicit, but never written out in this simple form, in the earlier work of Tribble.

(ii) A comparison of the synchrotron emissivity between uniform-field models and more realistic random-field models is particularly simple if we assume that the two have the same mean magnetic field energy density: in this case, we find that the mean emissivity is almost unchanged, a result that can be derived either from simple physical arguments or from integrating the synchrotron emissivity function over B. If the electron energy density scales as some power of the magnetic field strength, while retaining the same mean value, then the mean emissivity increases, but not by large factors. Standard minimum-energy arguments that rely on uniform-field assumptions for B are not wrong by large factors.

(iii) JP electron spectra in random fields give rise to a well-defined synchrotron spectrum (the 'TJP spectrum') that is significantly different from the standard JP synchrotron spectrum; I have presented a simple recipe for calculating this model numerically. The applicability of the TJP spectrum to real sources can be tested using fits to broad-band data from the current generation of radio telescopes. Numerical modelling shows that there may be very significant scatter in finite-sized realizations of this spectrum due to structure in the synchrotron emissivity. Fitting a TJP spectrum with a JP model may cause the low-frequency spectral index ('injection

index') to be overestimated and the spectral ages to be underestimated.

(iv) Random fields give rise to inverse-Compton emissivity which is generally very close to the expectation from uniform-field models: the energy densities in magnetic field estimated with the standard assumptions from inverse-Compton observations are therefore good estimates of the mean energy density, if the electron energy density is independent of field strength. If the electron energy density scales as some power s of the magnetic field strength, the field strength will be overestimated, but only by small factors for plausible values of s. The relationship between the resolved surface brightness of synchrotron and inverse-Compton emission depends on the value of s and this can in principle be tested by observations.

Harwood et al. (submitted) discuss fits of the TJP spectrum to real data, while Goodger et al. (in preparation) will attempt to constrain s from observations of resolved inverse-Compton emission. Applications of these models to the polarization of radio galaxies and their depolarization by the external medium will be discussed in a later paper.

ACKNOWLEDGEMENTS

This work has made use of the University of Hertfordshire Science and Technology Research Institute high-performance computing facility. I thank Judith Croston for helpful comments on a draft of the paper, and an anonymous referee for a constructive report which has helped to improve the paper.

REFERENCES

Alexander P., Leahy J. P., 1987, MNRAS, 224, 1
Blundell K. M., Rawlings S., 2000, AJ, 119, 1111
Brunetti G., 2000, Astropart. Phys., 13, 107
Burch S. F., 1977, MNRAS, 180, 623
Carilli C. L., Perley R. A., Dreher J. W., Leahy J. P., 1991, ApJ, 383, 554
Cho J., Lazarian A., 2003, MNRAS, 345, 325
Croston J. H., Hardcastle M. J., Birkinshaw M., 2005, MNRAS, 357, 279
Eilek J. A., 1989, AJ, 98, 244
Eilek J. A., 1996, in Hardee P. E., Bridle A. H., Zensus J. A., eds, ASP Conf. Ser. Vol. 100, Energy Transport in Radio Galaxies and Quasars. Astron. Soc. Pac., San Francisco, p. 281
Eilek J. A., Arendt P. N., 1996, ApJ, 457, 150
Eilek J. A., Melrose D. B., Walker M. A., 1997, ApJ, 483, 282
Fomalont E. B., Ebneter K. A., van Breugel W. J. M., Ekers R. D., 1989, ApJ, 346, L17
Goodger J. L., Hardcastle M. J., Croston J. H., Kassim N., Perley R. A., 2008, MNRAS, 386, 337
Hardcastle M. J., Croston J. H., 2005, MNRAS, 363, 649
Hardcastle M. J., Croston J. H., 2011, MNRAS, 415, 133
Hardcastle M. J., Birkinshaw M., Cameron R., Harris D. E., Looney L. W., Worrall D. M., 2002, ApJ, 581, 948
Hardcastle M. J., Harris D. E., Worrall D. M., Birkinshaw M., 2004, ApJ, 612, 729
Isobe N., Tashiro M., Makishima K., Iyomoto N., Suzuki M., Murakami M. M., Mori M., Abe K., 2002, ApJ, 580, L111
Isobe N., Makishima K., Tashiro M., Hong S., 2005, ApJ, 632, 781
Jaffe W. J., Perola G. C., 1973, A&A, 26, 423
Jamrozy M., Konar C., Machalski J., Saikia D. J., 2008, MNRAS, 385, 1286
Kaiser C. R., 2005, MNRAS, 360, 176
Kardashev N. S., 1962, Astronomy, 6, 317
Kataoka J., Stawarz Ł., 2005, ApJ, 622, 797
Katz-Stone D. M., Rudnick L., Anderson M. C., 1993, ApJ, 407, 549
Laing R. A., Bridle A. H., Parma P., Feretti L., Giovannini G., Murgia M., Perley R. A., 2008, MNRAS, 386, 657
Liu R., Pooley G. G., Riley J. M., 1992, MNRAS, 257, 545
Longair M. S., 2010, High Energy Astrophysics. Cambridge Univ. Press, Cambridge
Mack K.-H., Klein U., O'Dea C. P., Willis A. G., Saripalli L., 1998, A&A, 329, 431
Matthews A. P., Scheuer P. A. G., 1990a, MNRAS, 242, 616
Matthews A. P., Scheuer P. A. G., 1990b, MNRAS, 242, 623
Mendygral P. J., Jones T. W., Dolag K., 2012, ApJ, 750, 166
Murgia M., Fanti C., Fanti R., Gregorini L., Klein U., Mack K.-H., Vigotti M., 1999, A&A, 345, 769
Murgia M., Govoni F., Feretti L., Giovannini G., Dallacasa D., Fanti R., Taylor G. B., Dolag K., 2004, A&A, 424, 429 (M04)
Myers S. T., Spangler S. R., 1985, ApJ, 291, 52
Pacholczyk A. G., 1970, Radio Astrophysics. Freeman & Co., San Francisco
Rybicki G. B., Lightman A. P., 1979, Radiative Processes in Astrophysics. Wiley, New York
Swain M. R., Bridle A. H., Baum S. A., 1998, ApJ, 507, L29
Tregillis I. L., Jones T. W., Ryu D., 2001, ApJ, 557, 475
Tribble P. C., 1991, MNRAS, 253, 147
Tribble P. C., 1993, MNRAS, 261, 57
Tribble P. C., 1994, MNRAS, 269, 110

This paper has been typeset from a TEX/LATEX file prepared by the author.